Helical Gear Wear Monitoring: Modelling and Experimental Validation

Khaldoon F. Brethee[1, 2], Dong Zhen[3], Fengshou Gu[1], Andrew D. Ball[1]

[1]Centre for Efficiency and Performance Engineering, University of Huddersfield, Huddersfield, HD1 3DH.

[2]Engineering College, University of Anbar, Ramadi, Iraq.

[3]School of Mechanical Engineering, Hebei University of Technology, China.

Corresponding author Email: khaldoon.brethee@hud.ac.uk; khaldon77m@hotmail.com

Abstract

Gear tooth surface wear is a common failure mode. It occurs over relatively long periods of service nonetheless, it degrades operating efficiency and lead to other major failures such as excessive tooth removal and catastrophic breakage. To develop accurate wear detection and diagnosis approaches at the early phase of the wear, this paper examines the gear dynamic responses from both experimental and numerical studies with increasing extents of wear on tooth contact surfaces. An experimental test facility comprising of a back-to-back two-stage helical gearbox arrangement was used in a run-to-failure test, in which variable sinusoidal and step increment loads along with variable speeds were applied and gear wear was allowed to progress naturally. A comprehensive dynamic model was also developed to study the influence of surface wear on gear dynamic response, with the inclusion of time-varying stiffness and tooth friction based on elasto-hydrodynamic lubrication (EHL) principles. The model consists of an 18 degree of freedom (DOF) vibration system, which includes the effects of the supporting bearings, driving motor and loading system. It also couples the transverse and torsional motions resulting from time-varying friction forces, time varying mesh stiffness and the excitation of different wear severities. Vibration signatures due to tooth wear severity and frictional excitations were acquired for the parameter determination and the validation of the model with the experimental results. The experimental test and numerical model results show clearly correlated behaviour, over different gear sizes and geometries. The spectral peaks at the meshing frequency components along with their sidebands were used to examine the response patterns due to wear. The paper concludes that the mesh vibration amplitudes of the second and third harmonics as well as the sideband components increase considerably with the extent of wear and hence these can be used as effective features for fault detection and diagnosis.

Keywords: Fault detection; Fault diagnosis; Gear wear; Elasto-hydrodynamic lubrication; Numerical model; Vibration response.

1 Introduction

Helical gears are commonly employed for power transmissions in a wide range of industrial machines such as wind turbines, helicopters, marine power trains and motor vehicles. As these applications are often of high criticality, condition monitoring of gears has received significant attentions in recent years. Tooth surface wear is a common failure mode of transmission systems, that takes place over a long period of service time, it has a negative influence on the dynamic behaviour and vibration response of the gear train [1, 2]. The diagnosis of wears as early as possible can avoid catastrophic failures and improve system availability [3-5]. To enable an on-line health monitoring capability, vibration signature analysis has been widely used as an effective tool for machine diagnostic inference.

A wide number of dynamic models for various gearbox systems have been presented in [6-9], in which both torsional and translational vibration responses of gears were studied as a tool for aiding gear fault diagnosis. A variety of models have been developed for the diagnostics of different faults, such as gear spalling or tooth breakage [7, 10-12], tooth crack [13-16], shaft misalignment [17, 18], tooth surface pitting and wear [19-25]. More models have been developed to analyse the time varying mesh stiffness in a helical gear [26-30] and to study the effect of parametrical design on the dynamic behaviour of helical gear system [31-34]. Numerical models can be very valuable for gaining in-depth understanding of the complex interaction between transmission components, whereby effective methods to process vibration signals for implementing accurate and reliable diagnostics can be developed. However, few models have been presented for fault detection and diagnosis in helical gear systems, likely due to the increased complexity of time-varying contact lines during the meshing process.

Several studies have been performed to develop analytical methods for modelling helical gear stiffness. Kar and Mohanty[35, 36] suggested an algorithm for determination of the time-varying stiffness, time varying frictional force and torque between meshing teeth and the bearings in a helical gear system. This algorithm was revised and refined by Jiang et al. [37-39] to develop more accurate representations in stiffness variations of helical gears during the mesh process. They investigated the effect of spalling defect, tooth breakage and mesh misalignment on the helical gear dynamic features. Chang Q. et al. [40] used the same algorithm to develop a dimensionless method for studying the nonlinear characteristics of helical gear model. Maczak J. [41] presented a simulation model based on finite element method (FEM), for detection of local faults like pitting and tooth fracture in helical gears using abnormalities in the time vibration signal, whereas long computation time is required with FEM. A number of dynamic models of spur and helical gear systems incorporated with a wear formulation were studied by Ding H. [21, 42], in terms of gear design modifications. However, more

accurate models are needed to investigate the wear effect on helical gear dynamic performance for easier demonstrating and evaluating the condition monitoring perspective.

Numerous dynamic models of gear systems were incorporated with a generalized wear formulation to predict the interactions between the dynamic behaviour and tooth surface wear [20]. A family of dynamic models of spur and helical gear systems incorporated with a wear formulation based on Archard's wear model [24, 43-49] due to its simplicity, however it requires an experimental wear coefficient that is difficult to be determined as it depends on many aspects such as material properties, lubricants, surface quality, operating conditions [24]. In dynamic respect, the wear effect is mainly characterized by loss of tooth profile that represented by modulated mesh excitations [25, 50, 51], to investigate the effects of surface wear on system's dynamic characteristics. They indicated that tooth surface wear and gear dynamics are highly interacted, whereas tooth wear may cause unfavourable changes in the tooth surface topography and have a significant adverse effect on gear life and performance. However, limited number of contributions have been reported to include the combined influence of wear evolutions and vibrations for helical gears with respective to accuracy and easiness of implementation for condition monitoring and diagnostics for the early stages of wear. In addition, monitoring of gear wear based on vibration is not particularly well-established [52] and most of the models either ignore or assume constant frictional effects, which is likely to be very different from real applications where the load and hence the frictional forces vary during the meshing process.

Various models have been produced to evaluate the effect of sliding friction on spur and helical gear dynamic responses [53], based on FEM [54-56] and numerical modelling [57], using different values of the coefficient of friction. These have indicated that friction appears as a non-negligible excitation source, which can generate significant time-varying excitations and enhance the amplitudes of the lower and higher harmonics of the translational responses, which in turn can enhance conventional diagnostic features [58]. To date, few studies have focused on the diagnostics of tooth surface wear with the inclusion of frictional effects and most of the presented helical gear models have not been validated with the experimental work.

The main objective of this study is to develop a computationally efficient and stable analysis of the dynamic response of a helical gearbox for the purpose of condition monitoring. To this end, a numerical model is developed to simulate time-varying mesh stiffness, coupled with EHL frictional model and tooth wear characteristics, as a basis for increasing the accuracy of gear diagnostics by examining the changes in dynamic forces and the corresponding vibration responses under different degrees of tooth surface wear. The results obtained from the model is then validated by vibrations

acquired from a run-to-failure experimental approach. As a result, an accurate diagnostic model is presented to define effective indicator features of tooth surface wear defects.

2 Modelling Tooth Wear in Helical Gears

Gear wear results in deviation from gear tooth profile and thickness as well as altering load distributions and contact stresses, which can accelerate the occurrence of other failure modes such as pitting and scoring [20, 59]. Stiffness reduction is commonly used in dynamic gear mesh models to represent tooth surface defects [19, 60, 61].

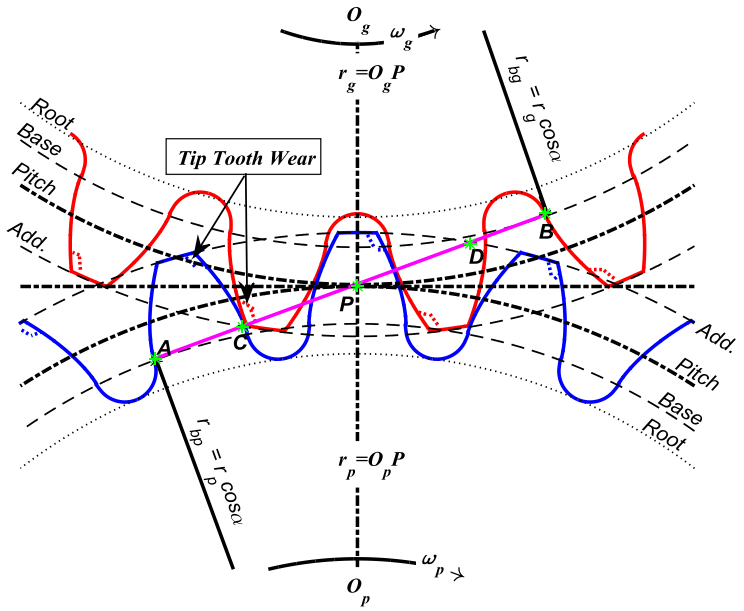

Figure 1 Gear mesh process of a single cross-sectional plane of helical gears with tooth wear

Tooth surface wear can cause sliding and the normal load amplitudes to vary with the position of the contact on the tooth surfaces, in turn this can cause difficulties with the computation of load distributions for the gears [62]. Wear tends to accumulate gradually with operation durations and may cause progressive change in the contact regions due to the tooth profile alterations [63]. As a result, the shape of the tooth is varying continuously due to the progressive effect of wear. Eventually, it influences the vibration behaviour because of changes in gear meshing parameters such as backlash, centre distance, tooth thickness, pressure angle etc. [64].

Figure 1 shows a single cross-sectional plane of a helical gear mesh with involute teeth whereby the contact points passing through the line of action (LOA) moves from point C to point D. A uniform

tooth surface wear is also shown, which gives an approximate explanation to the effect of wear on tooth pattern geometry. An increase in wear severity on tooth surface will enlarge the gear centre distance and the pressure angle, while the length of the LOA will be decreased [65]. This implies that gear stiffness will have a slighter decrease whereas the parametric excitation is severer in a gear dynamic system. As a consequence of wear, higher dynamic forces along with higher frictional effects will be induced during the meshing process.

2.1 Time-Varying Contact Length for Modelling Wear

The power transmission of helical gears produces radial, tangential and axial dynamic forces on the mesh points, which excite vibrations in these directions[66, 67]. To examine these dynamic forces, a coordinate system is arranged as shown in Figure 2 (a), in which the x-axis is aligned with the off-line of action (OLOA) and directed perpendicularly to the plane of action ($CD\bar{D}\bar{C}$), the y-axis is aligned to the line-of-action (LOA), which is perpendicular to both the shaft axis and x-axis, and finally the z-axis is aligned (axial) along the centreline of the shafts.

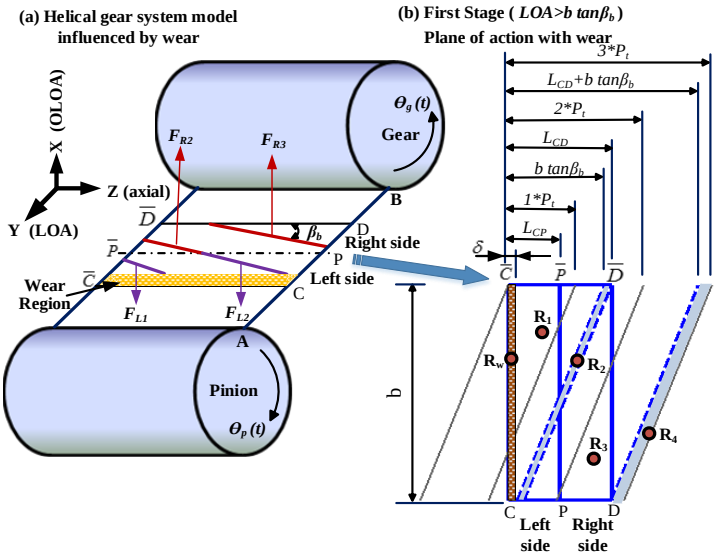

Figure 2 Equivalent plane of action of a helical gear system influenced by uniform wear

For healthy gears, the mesh cycle of three contacting pairs starts from point C and moves diagonally as the gears roll across the contact zone until point $\bar{D}$. However, uniform tooth wear will shift the starting point C and shorten the plane of action in proportion to the wear severity. This will affect the gear meshing stiffness, the contact surface friction and hence the gear vibration. The equivalent

frictional forces of each segment of the contact lines are also shown in Figure 2 (a). These forces influence the contact plane in two directions, on either side of the inclined pitch line ($P\bar{P}$).

To determine the contact line length between mating helical gears, the tooth face can be characterized with an analytical surface formula. It can be calculated at each instant of time by graphical or analytical methods. The region of contact is a rectangle of sides equal to tooth face width *b* and the length of the LOA (L_{CD}), which can generally be divided into different contact patterns as shown in Figure 2 (b), in this representation R_w is related to the wear region effect. During the progression of the mesh, the length of a single tooth pair increases gradually in region R_1, commencing at the root of one end of the tooth face, and then remaining constant in region R_2, after that it decreases in region R_3 and remains zero for some distance in region R_4. Moreover, the length of L_{CD} will be reduced by wear severity by an amount δ, which shortens the left side length as defined in Figure 2 (a) of the plane of action by an amount equal to the removal of material due to wear. The percentage of tooth wear was simulated as a ratio of the wear width δ to the length of the LOA (L_{CD}).

$$r_{\delta} = \frac{\delta}{L_{CD}} \tag{1}$$

The contact line is a function of gear geometric parameters and also depends on tooth face width and the length of LOA [35-37, 39]. For the case of $b\tan\beta_b > L_{CD}$ which is the case of the first stage gears for the gearbox, the time-varying contact length of each pair of meshing teeth can be calculated by taking into account the effect of tooth wear δ through a reduction of contact line in different mesh phases.

$$L_i(t) = \begin{cases} 0 & 0 \le DL_i(t) < \delta \\ (DL_i(t) - \delta)\csc\beta_b & \delta \le DL_i(t) < b\tan\beta_b + \delta \\ b\tan\beta_b \csc\beta_b & b\tan\beta_b + \delta \le DL_i(t) < L_{CD} \\ (L_{CD} + b\tan\beta_b - DL_i(t))\csc\beta_b & L_{CD} \le DL_i(t) < L_{CD} + b\tan\beta_b \\ 0 & L_{CD} + b\tan\beta_b \le DL_i(t) < n * P_t \end{cases} \tag{2}$$

where the variables can be specified according to the relationships in Figure 2:

$$DL_i(t) = \mathrm{mod}(r_{bp} \times \theta_{pi}, n \times P_t) \tag{3}$$

‘‘mod’’ is the modulus function defined as [68],

$$\mathrm{mod}(x, y) = x - y\ floor(x / y) \quad , \quad y \neq 0 \tag{4}$$

$$\theta_{pi} = \theta_p + (i-1)\, P_{angle} \tag{5}$$

$$P_t = 2\pi\, r_{bp} / z_1 \tag{6}$$

$$P_{angle} = 2\pi / z_1 \tag{7}$$

$$L_{CD} = LOA = \sqrt{r_{ap}^2 - r_{bp}^2} + \sqrt{r_{ag}^2 - r_{bg}^2} - (r_p + r_g)\sin\alpha_t \tag{8}$$

θ_p is the pinion rotational angle, P_{angle} and P_t denote the pitch duration angle and the circular transverse base pitch of the gear teeth respectively. The number of contact pairs is denoted as $i=1, 2, \ldots, n$, whereas n represents the maximum number of contact teeth, which is the upwards rounding of the number of contact pairs, $n=ceil(\varepsilon_{a1}+\varepsilon_{b1})$. Also, r_{bp} is the base radius of the pinion, r_{ap} is the addendum radius of the pinion, r_{ag} and r_{bg} are the addendum and base radius of the gear, r_p and r_g are the pitch circle radius of the pinion and gear respectively, whereas β_b and α_t are the base helical angle and transverse pressure angle respectively.

As previously mentioned, the length of each contact line increases gradually from the root of one end of the tooth face and then remains constant before decreasing to zero, and because of this then the total of the contact lines is the summation of the instantaneous contact lines of the teeth pairs in the mesh cycle:

$$L_{sum}(t) = \sum_{i=1}^{n} L_i\,(t) \tag{9}$$

which can be illustrated in Figure 3. It shows that the contact lines exhibit a periodic variation with angular displacement of the pinion gear. Such variations will induce time-varying frictional excitations in meantime they cause the time variations in gear mesh stiffness and damping variations [36].

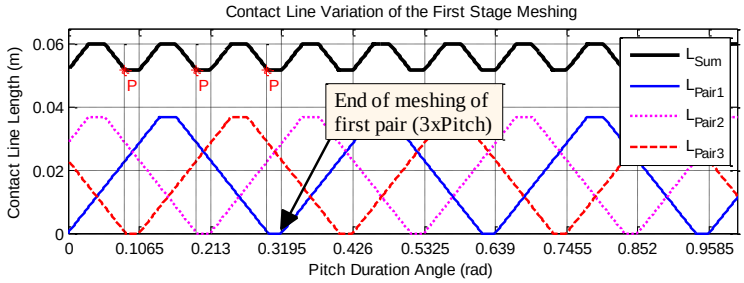

Figure 3 Length variations of the normal first stage contact lines

2.2 Effect of Wear on Time Varying Mesh Stiffness

To investigate the effects of surface wear on system's dynamic characteristics, the wear effect is modelled by the loss of tooth profile as that of [25, 50, 51], which is much easier to be implemented. Moreover, the material loss on the tooth surface is more uniformly in the early or mild wear phases. The uniform tooth wear adopted for the helical gears is considered to be more realistic for early operations as the gear operating conditions are under a relatively wide range in which the stress distribution spread more widely across tooth surfaces and hence uniform material removes, provided that gear meshes under adequate lubrication, high quality surface finishing and high quality of surface contact [22, 43, 45, 47]. In addition, tooth wear also reduces slightly the thickness of the tooth and increases the roughness of the surfaces, which can all induce a reduction in stiffness.

Dynamic measurements have verified that the mesh stiffness of a helical gear is roughly proportional to the sum of the lengths of the contact lines of all the tooth pairs in contact [69]. The contact line for a helical gear pair can be determined from the kinematic compatibility between the numerically generated surfaces of the teeth in contact, as expressed by Kar and Mohanty [35, 36] and subsequently modified by Jiang [37, 39]. The number of contact lines present in the contact zone depends upon the basic parameters of the gears, such as the normal module, the helix angle, the face width and the transmission ratio.

The summation of the lengths of the contact lines can be used as an alternative method to identify the varying mesh stiffness of helical gears [35-39], which is otherwise difficult to obtain due to the complexity of the contact geometry. The overall stiffness function is defined as a combination of the total length of the contact lines and a constant mesh stiffness density per unit length along the contact lines, as expressed in the ISO Standard Number 6336 [39, 57].

$$K_{mi}(t) = k_o \, L_i(t) \tag{10}$$

where k_o is the mesh stiffness density per unit length, which is calculated by the combination of bending stiffness k_b, shear stiffness k_s and axial compressive stiffness k_a with the Hertzian contact stiffness k_h and the tooth root fillet stiffness k_f of one slice of the tooth pair, which can be calculated as [15, 70]:

$$k_o = \frac{1}{\frac{1}{dk_h}+\frac{1}{dk_{b1}}+\frac{1}{dk_{s1}}+\frac{1}{dk_{a1}}+\frac{1}{dk_{f1}}+\frac{1}{dk_{b2}}+\frac{1}{dk_{s2}}+\frac{1}{dk_{a2}}+\frac{1}{dk_{f2}}} \tag{11}$$

where, the subscripts 1, 2 denote the pinion and gear, respectively. However, the gear mesh stiffness is influenced by worn tooth surfaces, as reflected in the reduction in tooth stiffness. Due to this decrease, the gear mesh stiffness is itself decreased and retarded angularly. The extent of subsequent tooth deflection depends upon the extent of tooth wear as illustrated in Figure 4 (a).

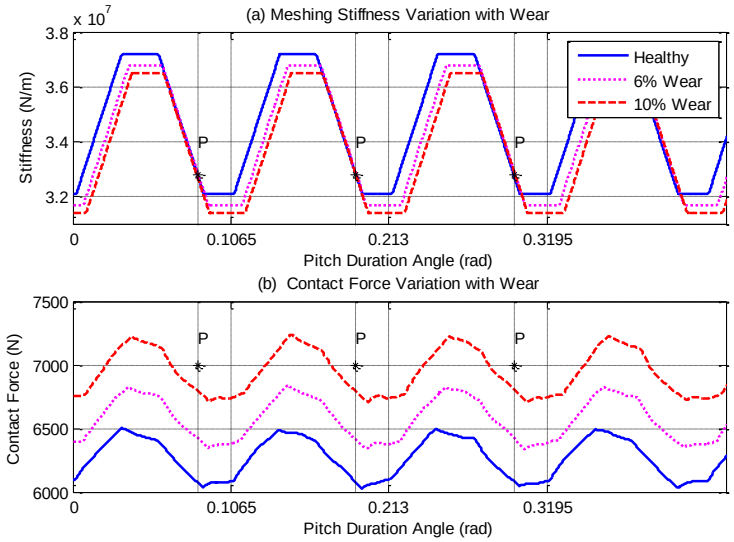

Figure 4 Time-varying mesh stiffness variations with different wear severities

As a consequence of tooth stiffness changes, a higher contact force will be produced for the same torque delivered at any given mesh position as shown in Figure 4 (b) according to [39]:

$$N_i(t) = K_{mi}(t)\,(r_{bp}\theta_p - r_{bg}\theta_g + y_p - y_g) + C_{mi}(t)\,(r_{bp}\dot{\theta}_p - r_{bg}\dot{\theta}_g + \dot{y}_p - \dot{y}_g) \tag{12}$$

$$C_{mi}(t) = 2\xi\sqrt{K_{mi}(t)\,I_e} \tag{13}$$

$$I_e = \frac{I_p I_g}{I_p r_{bg}^2 + I_g r_{bp}^2} \tag{14}$$

where $C_{mi}(t)$ is the meshing damping coefficient related to $K_{mi}(t)$, ξ is the damping ratio of the meshing teeth, I_e is the equivalent moment of inertia of the meshing gears and I_p, I_g are the inertia around the rotational axes of the pinion and the gear respectively.

2.3 Frictional Excitation

Friction force variation has fluctuates considerably along the meshing line and as such it is a considerable source of helical gear system excitation [40, 71]. To investigate more accurately the influence of gear lubricant parameters on dynamic response, a theoretical friction coefficient can be derived from elasto-hydrodynamic lubrication (EHL) and tribological theory [72] and in this study this was considered as the dominant mode of lubrication associated with the gear meshing surfaces. The friction representation formula used in this study was derived by Xu et al. [73], from experimental study and this can be used in a numerical simulation as a means of studying the process of EHL. The friction coefficient μ can be written:

$$\mu = e^{f(SR,P_h,\upsilon_o,S)} P_h^{b2} \left|SR\right|^{b3} V_e^{b6} v_0^{b7} R^{b8} \tag{15}$$

where

$$f(SR,P_h,\upsilon_o,S) = b1 + b4\left|SR\right| P_h \log_{10}(\upsilon_o) + b5e^{-\left|SR\right|P_h \log_{10}(\upsilon_o)} + b9e^{S} \tag{16}$$

In Xu's expressions, v_k and v_o are the kinematic and dynamic viscosities respectively of the lubricant EP320 that was used in the experimental test. P_h is the maximum Hertzian pressure, SR is the slide-to-roll ratio, V_e is the entrainment velocity and R is the combined radius of curvature. S is the root mean-square surface roughness (set such that S=0.07μm based on the manufacturing accuracy of the gear), which is the mean value used in [73]. The constant parameters: b1 … b9 are also used with the values proposed in the same reference.

Figure 5 (a) demonstrates the variation of friction coefficient based on an EHL model along the tooth profile of each contacting pair during the meshing process. The friction coefficient fluctuates periodically with the roll angle and is zero at its pitch point due to pure rolling motion. Tooth surface wear usually causes an increases in tooth surface roughness and hence further increase in friction between meshing teeth. For this reason, the EHL friction coefficient is increases with increasing wear as illustrated in Figure 5 (b).

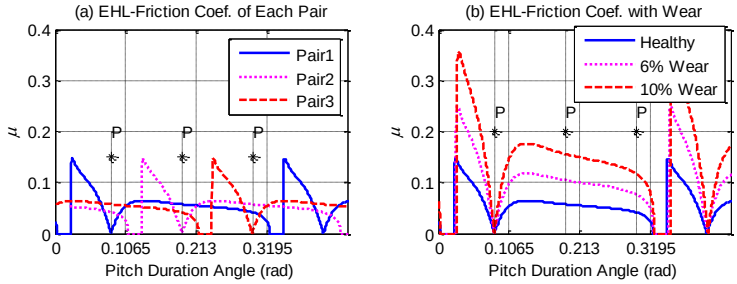

Figure 5 EHL friction coefficient of the first stage with wear

In the same way, tooth surface wear will result in higher moments about the gear centres and higher frictional forces in the translational motions of OLOA. As a consequence, additional noise and undesired vibrations are generated. In this study, the friction force is assumed to be uniformly distributed along the contact lines, hence splitting into two components with opposite directions as shown by F_{L1}, F_{L2}, F_{R2}, F_{R3} in Figure 2(a), which are perpendicular to the mesh plane. The right and left torque arms ($X_{ri}(t)$ and $X_{li}(t)$) of each friction force segment are obtained by taking the midpoint distance of each piece of the contact line length $L_{ri}(t)$ and $L_{li}(t)$ as explained in [37, 39]. Hence, the friction force of the i^{th} segment of the contact line at the meshing instance is given by:

$$F_{fi}(t) = \mu_i(t) \frac{N_i(t)}{L_{sum}(t)} (L_{ri}(t) - L_{li}(t)) \tag{17}$$

where $\mu_i(t)$ is the time varying friction coefficient based on the EHL model of each contact line and $N_i(t)$ is the normal resultant force of the stiffness and damping forces within the meshing contact. Moreover, the frictional torque of each contact line is determined from the moment formed by the friction force and the radius of curvature of each segment ($X_{ri}(t)$ and $X_{li}(t)$) as:

$$T_{fi}(t) = \mu_i(t) \frac{N_i(t)}{L_{sum}(t)} (L_{ri}(t) \times X_{ri}(t) - L_{li}(t) \times X_{li}(t)) \tag{18}$$

Hence, the total friction force and the torque of all of the engaged tooth pairs (n) can be found from:

$$\begin{aligned} F_f(t) &= \sum_{i=1}^{n} F_{fi}(t) \\ T_f(t) &= \sum_{i=1}^{n} T_{fi}(t) \end{aligned} \tag{19}$$

3 Numerical Analysis Based on a Two-Stage Helical Gearbox

An 18-DOF nonlinear model is proposed to simulate the dynamics of a two-stage helical gearbox system as shown in Figure 6. Each gear is represented by rigid blocks with four degrees of freedom (three translations and one rotation). The first and second stages of the gearbox are denoted with subscripts 1 and 2, and the pinion and gear wheels are denoted with subscripts p and g respectively. As shown by the geometric specification in Table 1, the chosen gear train system is a speed increaser, typical of that used in many industrial applications. The model includes six inertias, one each for the load motor, drive motor, two pinions and two gears, the latter four are denoted for the two stages of the gearbox using subscripts p1, g1, p2 and g2.

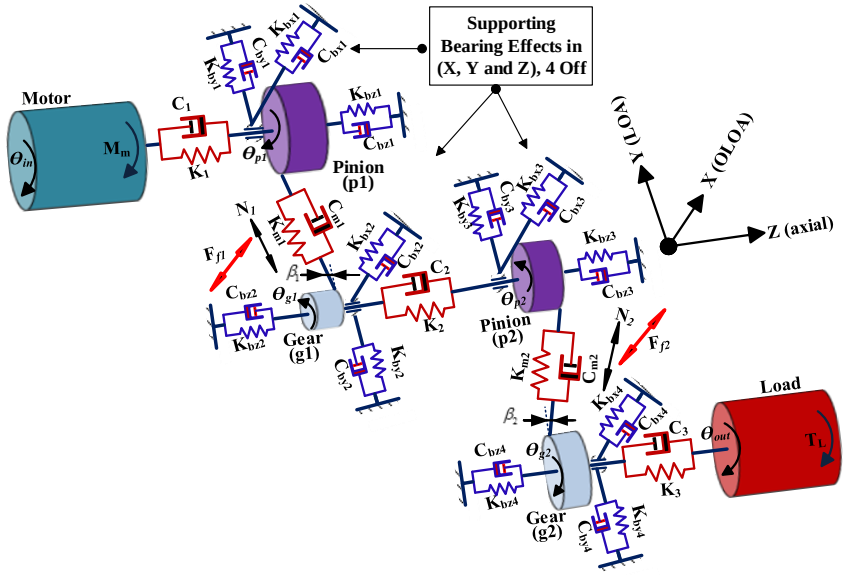

Figure 6 Two-stage helical gearbox system model

To represent an accurate gear transmission system, the model takes into account the effects of the speed-torque characteristics of both the driving and loading motor systems. The torsional compliances (stiffness and damping) of the shafts and the transverse compliances of supporting bearings are included in the model. The resilient elements of the supports are described by stiffness and damping coefficients as $K_{b\text{-}ij}$ and $C_{b\text{-}ij}$, the four bearings (i =1, 2, 3, 4) that in the j= x, y and z directions (i.e. LOA, OLOA and axial or shaft direction). The shafts between the system components are represented by torsional stiffness and torsional damping components K_1, K_2, K_3, C_1, C_2 and C_3. Furthermore, the model takes into account the influence of the driving torque and load torque T_m and T_L respectively.

Table 1 Geometric properties of the meshing gears

Geometric Properties	First Stage		Second Stage	
	Pinion	**Gear**	**Pinion**	**Gear**
Number of teeth	Z_{p1}=59	Z_{g1}=13	Z_{p2}=47	Z_{g2}=58
Pitch radius (mm)	r_{p1}=56.7	r_{g1}=12.5	r_{p2}=30.5	r_{g2}=37.6
Mass (kg)	m_{p1}=3.62	m_{g1}=0.4	m_{p2}=0.58	m_{g2}=0.9
Rotation speed (rpm)	203.74	924.66	924.66	749.3
Gear ratio	4.5384		0.81034	
Helix angle (°)	β_1=13		β_2=27	
Pressure angle (°)	ϕ=20		ϕ=20	
Module (mm)	M_1=2		M_2=1.25	
Working face width (mm)	b_1=36		b_2=25	
Transverse contact ratio	ε_{a1}=1.521		ε_{a2}=1.669	
Overlap contact ratio	ε_{b1}=1.289		ε_{b2}=2.89	

The equations of motion were represented in the state space form and then solved using the MATLAB ODE solver. The governing equations of motion for the model, depicted in Figure 6, were derived with the following assumptions:

- The pinion and gear are modelled as rigid disks;
- Input torque and load torque are applied to the system;
- Shaft mass and inertia are lumped with the gears;
- An EHL model is used to simulate the time variation of the friction coefficient μ;
- The helical gear teeth are assumed to be perfectly involute, manufacturing and assembly errors are ignored;
- Backlash is not considered in the model as gears are undertaking static loads.

According to Newton's laws of motion, the governing equations can be derived for the rotation of the motor rotor, the rotations of the pinions and gears of the two transmission stages, the rotation of the load rotor, and the translations for all rotors in the Y-direction (LOA), the Z-direction (axial) and the X-direction (OLOA), as presented in Equations from Eq. (20) to Eq. (38) respectively:

$$I_m\ddot{\theta}_{in}+c_1\left(\dot{\theta}_{in}-\dot{\theta}_{p1}\right)+k_1\left(\theta_{in}-\theta_{p1}\right)=M_m \tag{20}$$

$$\begin{aligned} &I_{p1}\ddot{\theta}_{p1}-c_1\left(\dot{\theta}_{in}-\dot{\theta}_{p1}\right)-k_1\left(\theta_{in}-\theta_{p1}\right)+r_{bp}C_{m1}(t)\left(r_{bp1}\dot{\theta}_{p1}-r_{bg1}\dot{\theta}_{g1}+\dot{y}_{p1}-\dot{y}_{g1}\right)\\ &+r_{bp1}K_{m1}\left(t\right)\left(r_{bp1}\theta_{p1}-r_{bg1}\theta_{g1}+y_{p1}-y_{g1}\right)+T_{fp1}=0 \end{aligned} \tag{21}$$

$$\begin{aligned} &I_{g1}\ddot{\theta}_{g1}+c_2\left(\dot{\theta}_{g1}-\dot{\theta}_{p2}\right)+k_2\left(\theta_{g1}-\theta_{p2}\right)-r_{bg1}C_{m1}(t)\left(r_{bp1}\dot{\theta}_{p1}-r_{bg1}\dot{\theta}_{g1}+\dot{y}_{p1}-\dot{y}_{g1}\right)\\ &-r_{bg1}K_{m1}\left(t\right)\left(r_{bp1}\theta_{p1}-r_{bg1}\theta_{g1}+y_{p1}-y_{g1}\right)-T_{fg1}\left(t\right)=0 \end{aligned} \tag{22}$$

$$I_{p2}\ddot{\theta}_{p2}-c_2\left(\dot{\theta}_{g1}-\dot{\theta}_{p2}\right)-k_2\left(\theta_{g1}-\theta_{p2}\right)+r_{bp2}C_{m2}(t)\left(r_{bp2}\dot{\theta}_{p2}-r_{bg2}\dot{\theta}_{g2}+\dot{y}_{p2}-\dot{y}_{g2}\right)$$
$$+r_{bp2}K_{m2}(t)\left(r_{bp2}\theta_{p2}-r_{bg2}\theta_{g2}+y_{p2}-y_{g2}\right)+T_{fp2}=0 \tag{23}$$

$$I_{g2}\ddot{\theta}_{g2}+c_3\left(\dot{\theta}_{g2}-\dot{\theta}_{out}\right)+k_3\left(\theta_{g2}-\theta_{out}\right)-r_{bg2}C_{m2}(t)\left(r_{bp2}\dot{\theta}_{p2}-r_{bg2}\dot{\theta}_{g2}+\dot{y}_{p2}-\dot{y}_{g2}\right)$$
$$-r_{bg2}K_{m2}(t)\left(r_{bp2}\theta_{p2}-r_{bg2}\theta_{g2}+y_{p2}-y_{g2}\right)-T_{fg2}(t)=0 \tag{24}$$

$$I_L\ddot{\theta}_{out}-c_2\left(\dot{\theta}_{g2}-\dot{\theta}_{out}\right)-k_1\left(\theta_{g2}-\theta_{out}\right)=-T_L \tag{25}$$

$$m_{p1}\ddot{y}_{p1}+C_{m1}(t)\cos\beta_{b1}\left(r_{bp1}\dot{\theta}_{p1}-r_{bg1}\dot{\theta}_{g1}+\dot{y}_{p1}-\dot{y}_{g1}\right)+K_{m1}(t)\cos\beta_{b1}(r_{bp1}\theta_{p1}-r_{bg1}\theta_{g1}$$
$$+y_{p1}-y_{g1})+C_{by1}\dot{y}_{p1}+K_{by1}y_{p1}=0 \tag{26}$$

$$m_{g1}\ddot{y}_{g1}-C_{m1}(t)\cos\beta_{b1}\left(r_{bp1}\dot{\theta}_{p1}-r_{bg1}\dot{\theta}_{g1}+\dot{y}_{p1}-\dot{y}_{g1}\right)-K_{m1}(t)\cos\beta_{b1}(r_{bp1}\theta_{p1}-r_{bg1}\theta_{g1}$$
$$+y_{p1}-y_{g1})+C_{by2}\dot{y}_{g1}+K_{by2}y_{g1}=0 \tag{27}$$

$$m_{p2}\ddot{y}_{p2}+C_{m2}(t)\cos\beta_{b2}\left(r_{bp2}\dot{\theta}_{p2}-r_{bg2}\dot{\theta}_{g2}+\dot{y}_{p2}-\dot{y}_{g2}\right)+K_{m2}(t)\cos\beta_{b2}(r_{bp2}\theta_{p2}-r_{bg2}\theta_{g2}$$
$$+y_{p2}-y_{g2})+C_{by3}\dot{y}_{p2}+K_{by3}y_{p2}=0 \tag{28}$$

$$m_{g2}\ddot{y}_{g2}-C_{m2}(t)\cos\beta_{b2}\left(r_{bp2}\dot{\theta}_{p2}-r_{bg2}\dot{\theta}_{g2}+\dot{y}_{p2}-\dot{y}_{g2}\right)-K_{m2}(t)\cos\beta_{b2}(r_{bp2}\theta_{p2}-r_{bg2}\theta_{g2}$$
$$+y_{p2}-y_{g2})+C_{by4}\dot{y}_{g2}+K_{by4}y_{g2}=0 \tag{29}$$

$$m_{p1}\ddot{z}_{p1}+C_{m1}(t)\sin\beta_{b1}[\dot{z}_{p1}-\dot{z}_{p1}+\tan\beta_{b1}(r_{bp1}\dot{\theta}_{p1}-r_{bg1}\dot{\theta}_{g1}+\dot{y}_{p1}-\dot{y}_{g1})]$$
$$+K_{m1}(t)\sin\beta_{b1}[z_{p1}-z_{g1}+\tan\beta_{b1}(r_{bp1}\theta_{p1}-r_{bg1}\theta_{g1}+y_{p1}-y_{g1})]+C_{bz1}\dot{z}_{p1}+K_{bz1}z_{p1}=0 \tag{30}$$

$$m_{g1}\ddot{z}_{g1}-C_{m1}(t)\sin\beta_{b1}[\dot{z}_{p1}-\dot{z}_{p1}+\tan\beta_{b1}(r_{bp1}\dot{\theta}_{p1}-r_{bg1}\dot{\theta}_{g1}+\dot{y}_{p1}-\dot{y}_{g1})]$$
$$-K_{m1}(t)\sin\beta_{b1}[z_{p1}-z_{g1}+\tan\beta_{b1}(r_{bp1}\theta_{p1}-r_{bg1}\theta_{g1}+y_{p1}-y_{g1})]+C_{bz2}\dot{z}_{g1}+K_{bz2}z_{g1}=0 \tag{31}$$

$$m_{p2}\ddot{z}_{p2}+C_{m2}(t)\sin\beta_{b2}[\dot{z}_{p2}-\dot{z}_{p2}+\tan\beta_{b2}(r_{bp2}\dot{\theta}_{p2}-r_{bg2}\dot{\theta}_{g2}+\dot{y}_{p2}-\dot{y}_{g2})]+K_{m2}(t)\sin\beta_{b2}$$
$$[z_{p2}-z_{g2}+\tan\beta_{b2}(r_{bp2}\theta_{p2}-r_{bg2}\theta_{g2}+y_{p2}-y_{g2})]+C_{bz3}\dot{z}_{p2}+K_{bz3}z_{p2}=0 \tag{32}$$

$$m_{g2}\ddot{z}_{g2}-C_{m2}(t)\sin\beta_{b2}[\dot{z}_{p2}-\dot{z}_{p2}+\tan\beta_{b2}(r_{bp2}\dot{\theta}_{p2}-r_{bg2}\dot{\theta}_{g2}+\dot{y}_{p2}-\dot{y}_{g2})]-K_{m2}(t)\sin\beta_{b2}$$
$$[z_{p2}-z_{g2}+\tan\beta_{b2}(r_{bp2}\theta_{p2}-r_{bg2}\theta_{g2}+y_{p2}-y_{g2})]+C_{bz4}\dot{z}_{g2}+K_{bz4}z_{g2}=0 \tag{33}$$

$$m_{p1}\ddot{x}_{p1}+C_{bx1}\dot{x}_{p1}+K_{bx1}x_{p1}-F_{f1}=0 \tag{34}$$

$$m_{g1}\ddot{x}_{g1}+C_{bx2}\dot{x}_{g1}+K_{bx2}x_{g1}+F_{f1}=0 \tag{35}$$

$$m_{p2}\ddot{x}_{p2} + C_{bx3}\dot{x}_{p2} + K_{bx3}x_{p2} - F_{f2} = 0 \quad (36)$$

$$m_{g2}\ddot{x}_{g2} + C_{bx4}\dot{x}_{g2} + K_{bx4}x_{g2} + F_{f2} = 0 \quad (37)$$

As these coupled equations are nonlinear, a numerical solution was derived to study the vibration responses under different conditions. A Runge–Kutta algorithm, with a fixed time step, was used to integrate the governing differential equations to produce the time domain responses of the system, in line with the time varying mesh stiffness and the EHL frictional excitations. The initial conditions were set to the steady state values for the rotational variables and zeros for the translations. In this way the solutions converged to a constant speed of interest after a short transient process.

4 Validation Tests

To validate the model, a number of vibration datasets were obtained from a run-to-failure gear test. The test was based on a representative two-stage helical gearbox test system as shown in Figure 7. The system consists of two industrial gearboxes installed back-to-back in series. The first gearbox is driven by an AC drive motor, and acts as a speed reducer, whilst the second gearbox is a speed increaser connected to a DC loading motor. Both gearboxes have two stage helical gears as detailed in Table 1, with a gear ratio of 3.678 and a rated power of 13.1 kW. The rig is driven by 15 kW AC motor at 1460 rpm while a DC motor/generator used to apply different loads. A closed loop control system, as depicted in Figure 8, was used for setting up the required operating conditions of the test rig via a touch screen interface which enabled the control of overall test duration, speed, load and number of operating cycles within a load setting.

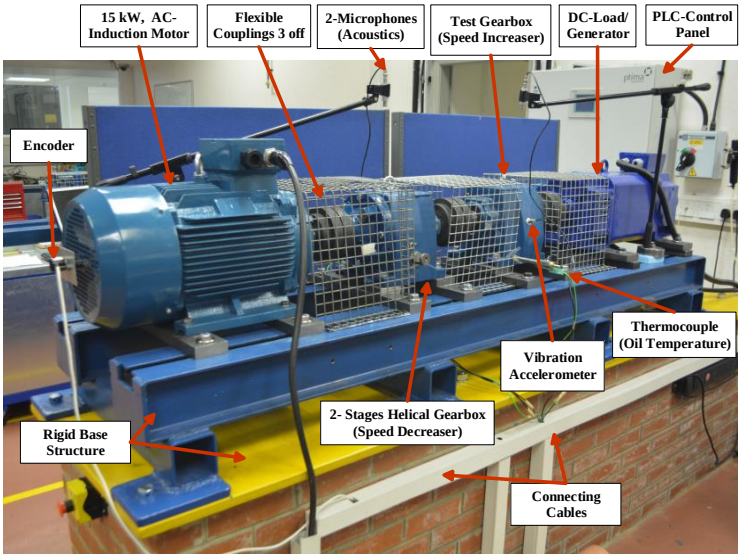

Figure 7 Test rig construction

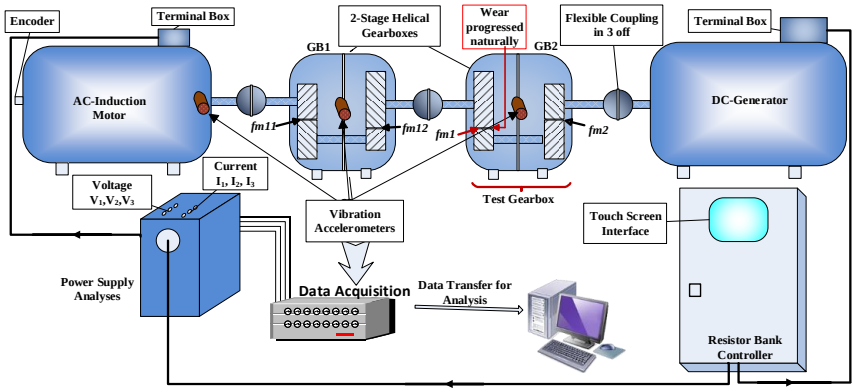

Figure 8 A schematic diagram of the test rig system (GB1 stands for gearbox 1; GB2 stands for gearbox 2; *fm11* and *fm12* are the mesh frequencies of each stage in GB1; *fm1* and *fm2* are the mesh frequencies of each stage in the test gearbox (GB2))

To simulate variable load operating scenarios experienced by wind turbine and helicopter gearboxes [74, 75], different operating loads and speeds were applied to the system, whereby the test rig operated for more than 800 hours under two different loading regimes: sinusoidal variable load which fluctuates at a frequency of 0.077 Hz, from 0 up to 12.5 kW with 1038rpm speed (70% of rated speed) followed by an increasing 25% stepped load at 70% and 50 % rated speed, the total test time being 60 minutes, as illustrated in Figure 9.

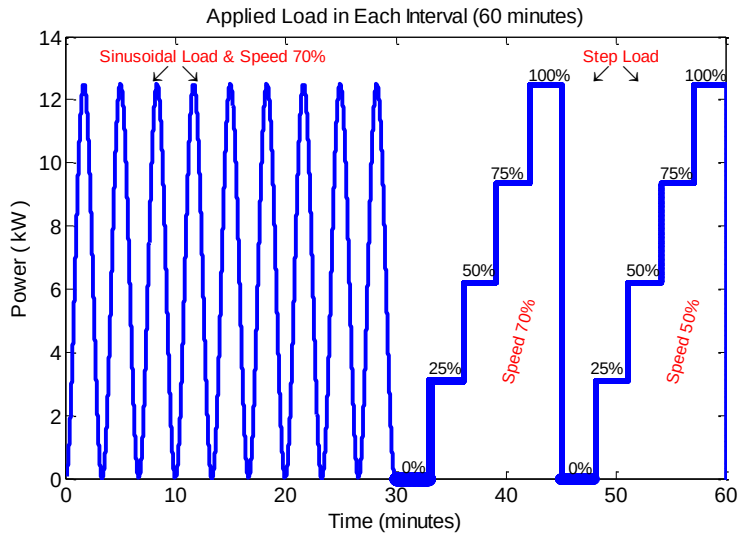

Figure 9 Sinusoidal and stepped load regimes of the experiment test

During the test, the online monitoring system was recorded the change in the three mesh harmonics and associated sidebands for each stage, obtained from the amplitude spectrum of the time synchronous averaged (TSA) vibration signals. The test was terminated when vibration sideband features exhibited a significant increase (higher than twice their baselines), showing an existence of a considerable fault in the test gearbox. Figure 10 illustrates the gear wear defects in the first stage of the test gearbox after the test was terminated. It can be seen that, the significant surface scuffing due to the wear affects both the pinion and gear tooth surfaces by almost the same size severity, showing the gears are considerably faulty. The worn regimes are in the late stage of tooth surface wear, in which the surface wear and mild wear are more realistic for early operations and very early stages of wear, that commonly happen due to metallurgical defects in gear material, improper heat treatment, improper surface finish and manufacturing error. To diagnose the tooth surface wear in its early stages, a uniform wear model was simulated in the dynamic model, whereas the small amount of wear and uniform material removes can be demonstrated and assessed effectively for the condition monitoring scheme.

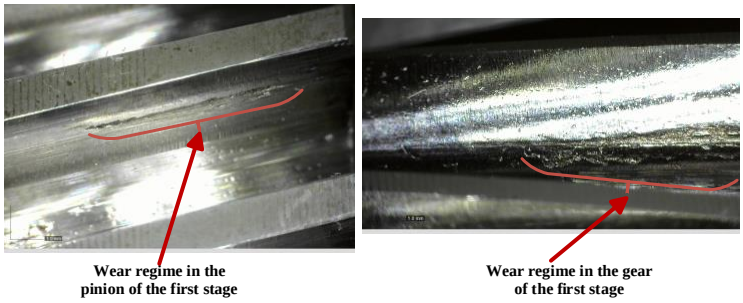

Figure 10 Illustrative photography of gear wear defects

5 Discussion

Different degrees of wear (from 0% to 10% of the tooth thickness, see Figure 2) were simulated in the model in steps of 2% to obtain features for wear fault diagnosis at an early stage in its development. The dynamic responses of the model were obtained in terms of the displacement, velocity and acceleration of the gear system under healthy and faulty conditions. Seven data sets (each of duration 1hour) were selected from across the final five hundred operating hours, as illustrated in Figure 11.

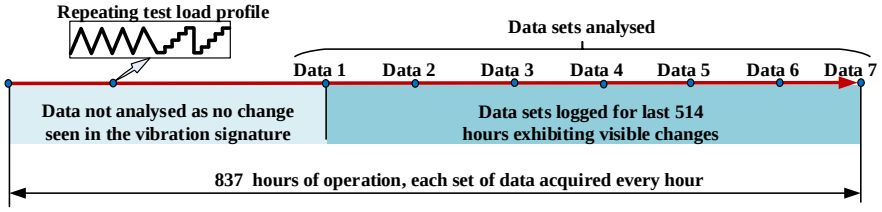

Figure 11 A schematic diagram of the experimental scenario illustrates the selected tests

5.1 Signals in the Time and Frequency Domains

Commented [s1]:

The tooth surface wear was found to affect the dynamic signals of the gearbox, resulting in higher vibration and noise. Time-domain analysis can be used as an effective indicator of the impulsive vibration of gear faults [11], but the spectrum is also commonly used for monitoring machine vibration characteristics. So, the numerical solutions were converted into accelerations by differentiating the velocity responses, which themselves had been derived from time data using the FFT.

In addition, to implement an effective means of detecting wear, time synchronous averaging (TSA) was applied to the experimental test data, TSA can suppress the influences of noise, which are

asynchronous to those features of interest [76]. Figure 12 (a) shows the time domain vibration responses after applying TSA to the experimental raw data, whereas Figure 12 (b) demonstrates the translational responses in the LOA direction acquired from the model when influenced by different wear severities. It can be seen that, depending on the extent of wear, higher impulsive vibration responses and higher amplitudes feature in both the experimental and model predicted signals of the gear meshing process. However, limited excitations can be identified in the numerical data with increasing the wear percentage because the model was developed to study the tooth surface wear at its early stage degrees and it does not take into account other potential excitations such as backlash, eccentricity, unbalance, run-out errors that can become severer as with the progression of wear and induce more vibrations. Although many studies have been carried out, those effect of gear imperfection with gear determinations still remains opening and a challenging task.

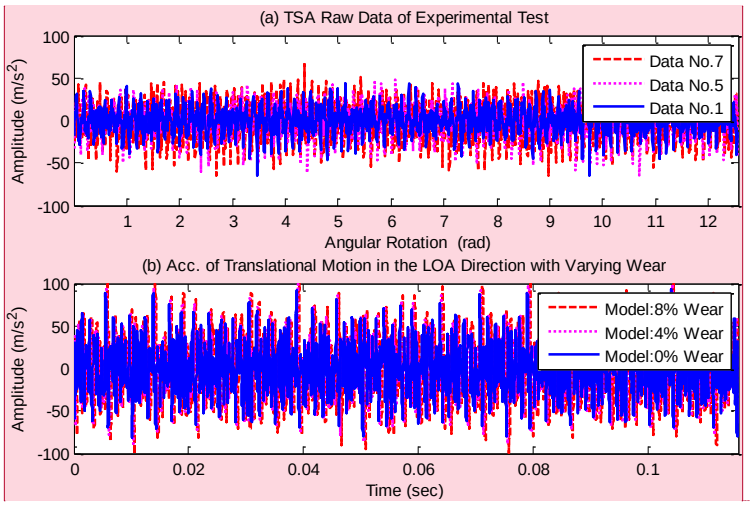

Commented [s2]: (a)TSA signal of measured acceleration (b)(b) Acceleration of model predicted

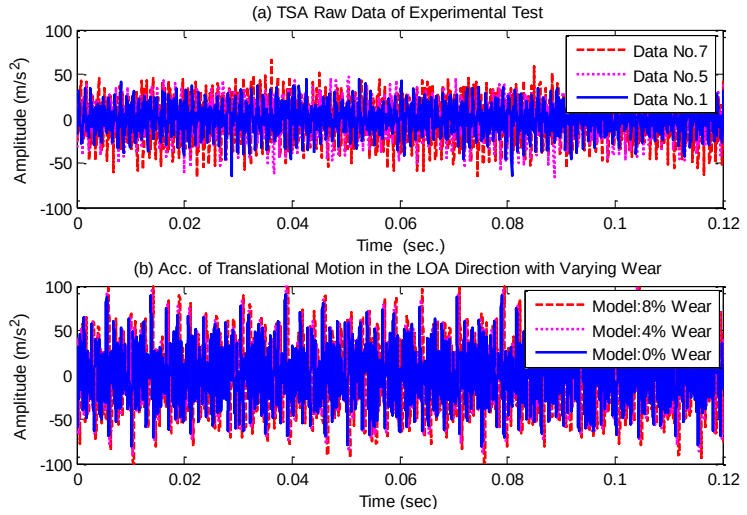

Figure 12 Experimental and numerical raw data of the gearbox under different wear severities

Spectrum analysis is commonly used for monitoring and interpreting the information contained in machine vibration characteristics, and the general behaviour of the vibration spectrum is illustrated in **Error! Reference source not found.** for the experimental and numerical data. To enhance the vibration signal features, TSA was used to extract a deterministic signal for vibration components

related to the rotational frequency of the target gear, and to reduce non-synchronous components and noise. The gear meshing frequencies and their components (up to 3rd harmonics) are shown. It can be seen that the meshing frequencies and their harmonics exhibit the similar trends between the experimental and model-predicted data, underlining that, the model response is simulated effectively.

The amplitudes at the meshing harmonics are not predicted as closely as would have been liked, possibly because of signal attenuation and noise in the experimental data and resonance effects in the vibration transmission paths. Especially, the transmission path alters more to the amplitudes at the high frequency range. As shown Figure 13(c), the frequency response function (FRF) exhibit higher magnitudes around 2,200Hz due to housing resonances. This makes the spectral peaks at and around $3\times f_{m2}$ particularly higher, as shown in Figure 13 (a).

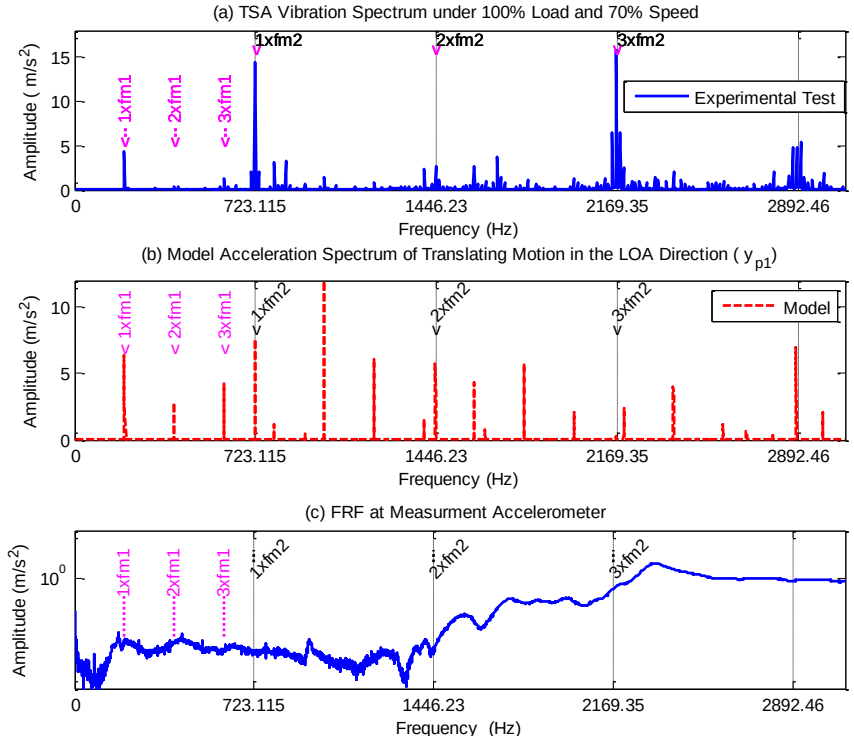

Figure 13 FRF signal of the tested gearbox based on impact hammer test (components for 70% speed)

5.2 Vibration at Meshing Frequencies

Existing studies have reported that tooth surface wear would lead to increases in the amplitude of tooth meshing harmonics, whereas the amplitude variations of higher order meshing harmonics can introduce useful and reliable information in detecting gear wear at its early stage [77, 78]. To diagnose gear condition, the spectral peaks up to the third tooth mesh harmonics of the 1st and 2nd stage meshing frequencies for the experimental results and the combined translational responses of the numerical model are represented in Figure 14 and Figure 15. It can be seen that the 2nd and 3rd harmonics of the mesh component ($f_{m1}=f_{r1}\times Z_{p1}$) associated with the first stage show a clear and consistent increase in spectral amplitude with developing of wear severity, under different operating load conditions, and for both the experimental and EHL model results. The selected experimental data sets show that the amplitudes at the 2nd and 3rd harmonics of the meshing frequency increase by more than 50%.

The 2nd harmonic peaks show that under 100% load, the vibration level at 70% speed is lower than 50% speed as illustrated in Figure 15 (c). This could be because of the nonlinearity effect of the contact process, in which the high load can change the hertz contact deformation and the contact stiffness that implemented between the meshing teeth. Moreover, resonance can be another possible parameter that result in higher excitation within a particular frequency range.

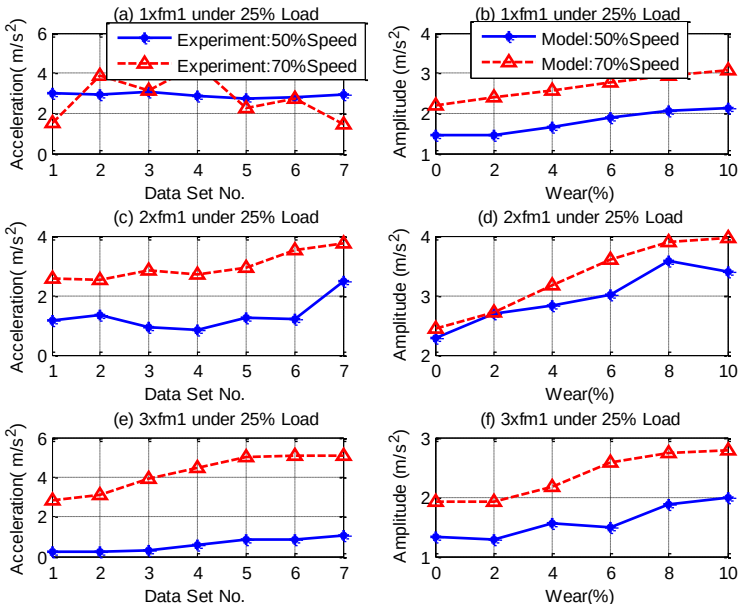

Figure 14 Spectral amplitudes of the first stage meshing components of the test gearbox under 25% load

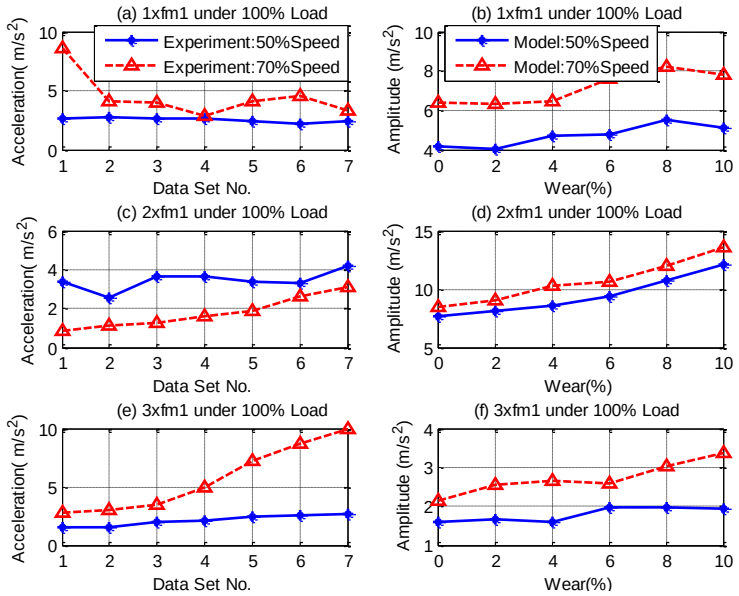

Figure 15 Spectral amplitudes at the first stage meshing components of the test gearbox under 100% load

Similarly, the predicted spectral peaks of the 2nd and 3rd harmonic components from the EHL model also clearly increase, but not generally by as much as 50% at 10% wear, which suggests that more tooth surface wear has happened between the gears. This could be due to the reversed friction force at the pitch point and/or to the fluctuating nature of the meshing process between two and three contact pairs. Evidently, these features can be considered as an effective indicator to diagnose wear severity between meshing gears. Hence, to identify tooth surface faults, the higher harmonics of the meshing frequency should be examined. By means of contrast, the amplitude of the vibration for the second stage meshing frequency components are illustrated in Figure 16 and Figure 17, for these un-worn gears there is no evident trend in either the experimental or model-predicted results.

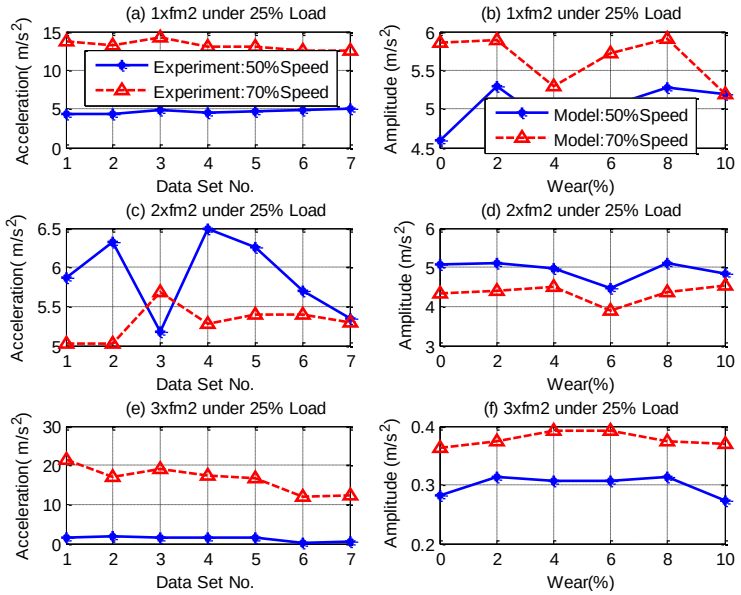

Figure 16 Spectral amplitudes of the second stage (healthy) meshing components of the test gearbox under 25% load

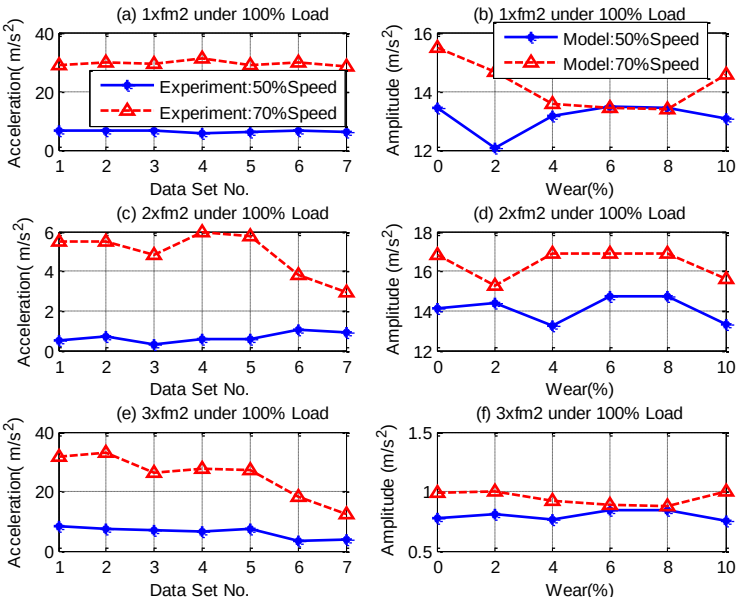

Figure 17 Spectral amplitudes of the second stage (healthy) meshing components of the test gearbox under 100% load

5.3 Vibration at Sideband Frequency

The difference in the vibration responses between healthy and faulty gears also causes changes in the sideband presence around the fundamental and harmonics of the gearbox meshing frequencies. The dynamic response computed with the analytical stiffness shows that the presence of sidebands arises from the amplitude modulation caused by the fall in stiffness [10]. The spectral amplitudes of the lower and upper sidebands ($f_{sb} = f_m \mp f_r$) around the first three harmonics of the first stage meshing frequency are shown in Figure 18 and Figure 19. It can be seen that the sideband peaks generally increase with wear for both experiment and model responses, with the most significant increase demonstrated by the higher sideband components. This is likely due to the non-linearity of the wear and friction between the tooth contact surfaces. The maximum difference increase between the selected experiment tests at the sideband components is about 100% for all harmonics.

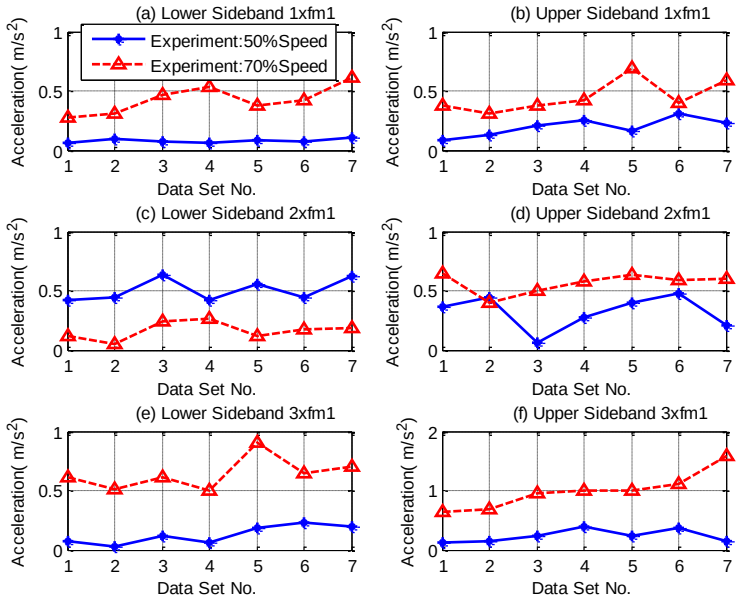

Figure 18 Experimental spectral amplitudes of the sidebands of the first stage meshing frequency components under 100% load

The spectral peaks for 10% tooth wear from the predictive model increase by approximately 50%, which also give a clear indication to the presence of wear. Sideband features can hence also provide useful information on the diagnostics of gear surface faults.

However, same nonlinearity effect can be illustrated in Figure 15 (c), which is consistent with the performance of the 2nd harmonic peaks (Figure 15 (c)). This could be due to the large inducing effect of resonance within this frequency range.

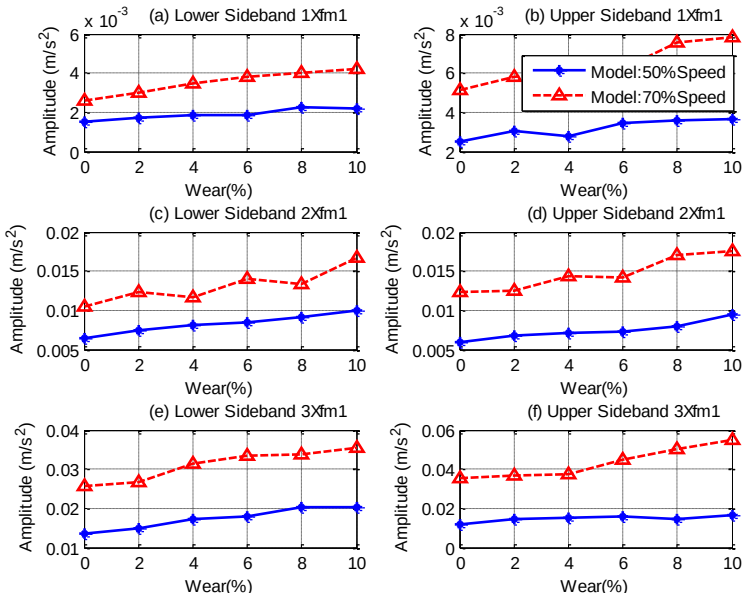

Figure 19 Predicted spectral amplitudes of the sidebands of the first stage meshing frequency components under 100% load

5.4 The Response to Wear with Different Gear Parameters

For further validation of the numerical model, different gear geometries were examined to explore the effect of tooth surface wear on meshing frequency components. Different tooth face widths and helix angles were simulated in the model with consideration of the effect that these changes have on the gear geometry parameters which affect the calculation of contact line length. Figure 20 shows the effect of wear on the meshing gear components for different tooth face widths.

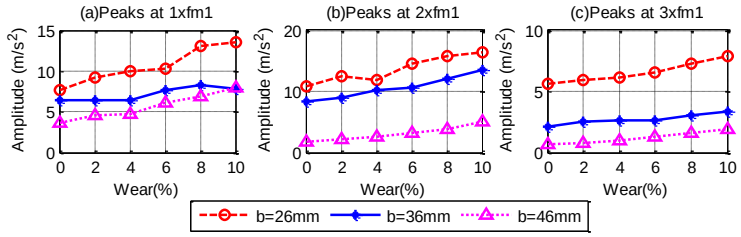

Figure 20 Spectral amplitudes of the first stage mesh frequency components with different tooth face widths (b)

From Figure 20, it can be seen that the 2nd and 3rd harmonics increase by more than 50% with 10% wear severity for a range of different tooth widths. A lower vibration level can be observed with decreasing tooth width, as a result of reduced frictional effects. The same trend behaviour with wear degree for low and high helix angles is identified at the 1st and 2nd harmonics of the mesh frequency as illustrated in Figure 21. However, the 3rd harmonic exhibits quadratic behaviour potentially because of reducing gear vibration with increasing helix angle.

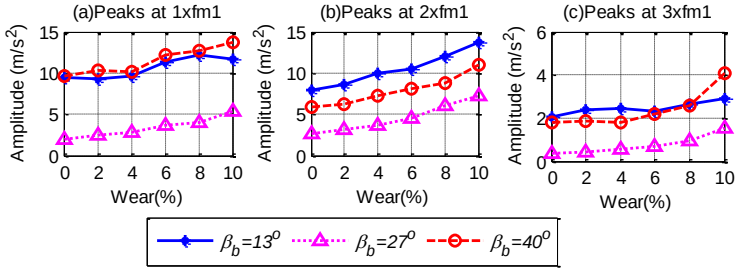

Figure 21 Spectral amplitudes of the first stage mesh frequency components with different base helix angles (β_b)

Conclusion

This paper investigates the changes in dynamic forces and corresponding vibration responses of an industrial two-stage helical gearbox under different degrees of tooth surface wear. The experimental dataset was obtained by a run-to-failure test, in which gear wear is naturally progressed over a time period of 837 hours. Simultaneously, a model was developed incorporating time-varying stiffness and tooth friction based on an elasto-hydrodynamic lubrication (EHL) model, and where the tooth wear of the helical gears was modelled by reduced mesh stiffness and increased frictional excitation. The comparison of the experimental and model-predicted results shows a high degree of correlation in the trend behaviour.

Spectral peaks of TSA signatures at the mesh frequency components along with their sidebands were used to explore the characteristics of the vibration response, in the light of wear and frictional excitations. The results show that spectral peaks at the 2nd and 3rd harmonics of the meshing frequency (and associated sideband frequencies) are influenced more significantly by increasing amount of wear. This attributes that friction induced dynamic forces change at least twice per mesh period. It is hence concluded that these components can be used as effective wear indicators for the detection and diagnosis of tooth surface deterioration.

Acknowledgment

The authors acknowledge the Higher Committee for Education Development in Iraq (HCED) and the University of Anbar for their supports. Also this research was supported by National Natural Science Foundation of China (Grant no. 51605133) and Hebei Science and Technology Projects of China (Grant no. 17394303D).

References

1. Wojnarowski, J. and V. Onishchenko, *Tooth wear effects on spur gear dynamics.* Mechanism and Machine Theory, 2003. **38**(2): p. 161-178.
2. Kuang, J. and A. Lin, *The effect of tooth wear on the vibration spectrum of a spur gear pair.* Journal of Vibration and Acoustics, 2001. **123**(3): p. 311-317.
3. Jayaswal, P., A. Wadhwani, and K. Mulchandani, *Machine fault signature analysis.* International Journal of Rotating Machinery, 2008. **(2008)**: p. 10.
4. Arunyanart, P., *Fault identification in drivetrain components using vibration signature analysis*. 2015, PhD, Thesis, The University of Akron.
5. Aherwar, A., *An Investigation on Gearbox Fault Detection Using Vibration Analysis Techniques a Review.* Australian Journal of Mechanical Engineering, 2012. **10**(2).
6. Bartelmus, W., *Mathematical modelling and computer simulations as an aid to gearbox diagnostics.* Mechanical Systems and Signal Processing, 2001. **15**(5): p. 855-871.
7. Begg, C.D., C.S. Byington, and K.P. Maynard. *Dynamic simulation of mechanical fault transition*. in *Proceedings of the 54th Meeting of the Society for Machinery Failure Prevention Technology, Virginia Beach, VA*. 2000.
8. Begg, C.D., et al. *Dynamics modeling for mechanical fault diagnostics and prognostics*. in *Maintenance and Reliability Conference (MARCON 99)*. 1999. Gatlinburg, Tennessee, May 10-12, 1999.
9. Van Khang, N., T.M. Cau, and N.P. Dien, *Modelling parametric vibration of gear-pair systems as a tool for aiding gear fault diagnosis.* technische mechanik, 2004. **24**: p. 3-4.
10. Chaari, F., et al., *Effect of spalling or tooth breakage on gearmesh stiffness and dynamic response of a one-stage spur gear transmission.* European Journal of Mechanics-A/Solids, 2008. **27**(4): p. 691-705.
11. Jia, S. and I. Howard, *Comparison of localised spalling and crack damage from dynamic modelling of spur gear vibrations.* Mechanical Systems and Signal Processing, 2006. **20**(2): p. 332-349.
12. Lu, D., X. Gong, and W. Qiao. *Current-based diagnosis for gear tooth breaks in wind turbine gearboxes*. in *Energy Conversion Congress and Exposition (ECCE), 2012 IEEE*. 2012. IEEE.
13. Tian, Z., M.J. Zuo, and S. Wu, *Crack propagation assessment for spur gears using model-based analysis and simulation.* Journal of Intelligent Manufacturing, 2012. **23**(2): p. 239-253.
14. Wu, S., M.J. Zuo, and A. Parey, *Simulation of spur gear dynamics and estimation of fault growth.* Journal of Sound and Vibration, 2008. **317**(3): p. 608-624.

15. Chen, Z. and Y. Shao, *Dynamic simulation of spur gear with tooth root crack propagating along tooth width and crack depth.* Engineering Failure Analysis, 2011. **18**(8): p. 2149-2164.
16. Mohammed, O.D., M. Rantatalo, and J.-O. Aidanpää, *Dynamic modelling of a one-stage spur gear system and vibration-based tooth crack detection analysis.* Mechanical Systems and Signal Processing, 2015. **54**: p. 293-305.
17. Jammal, A., et al. *An experimental study on high speed helical gears misalignments and dynamic behavior under random loading*. in *Mechanical and Aerospace Engineering (ICMAE), 2016 7th International Conference on*. 2016. IEEE.
18. Jiang, H., et al., *The influence of mesh misalignment on the dynamic characteristics of helical gears including sliding friction.* Journal of Mechanical Science and Technology, 2015. **29**(11): p. 4563-4573.
19. Choy, F., et al., *Analysis of the Effects of Surface Pitting and Wear on the Vibrations of a Gear Transmission System*. 1994, DTIC Document.
20. Ding, H., *Dynamic wear models for gear systems, PhD DISSERTATION*. 2007, The Ohio State University.
21. Ding, H., *A study of interactions between dynamic behavior of gear systems and surface wear*. 2007, The Ohio State University.
22. Flodin, A., *Wear of spur and helical gears.* Royal Institute of Technology, Stockholm, Doctoral Thesis, 2000.
23. Hu, C., et al., *Development of a gear vibration indicator and its application in gear wear monitoring.* Mechanical Systems and Signal Processing, 2016. **76**: p. 319-336.
24. Ding, H. and A. Kahraman, *Interactions between nonlinear spur gear dynamics and surface wear.* Journal of Sound and Vibration, 2007. **307**(3): p. 662-679.
25. Liu, X., Y. Yang, and J. Zhang, *Investigation on coupling effects between surface wear and dynamics in a spur gear system.* Tribology International, 2016. **101**: p. 383-394.
26. Wang, Q., et al., *Effects of different coupling models of a helical gear system on vibration characteristics.* Journal of Mechanical Science and Technology, 2017. **31**(5): p. 2143-2154.
27. Wang, Q. and Y. Zhang, *A model for analyzing stiffness and stress in a helical gear pair with tooth profile errors.* Journal of Vibration and Control, 2015: p. 1077546315576828.
28. Hedlund, J. and A. Lehtovaara, *A parameterized numerical model for the evaluation of gear mesh stiffness variation of a helical gear pair.* Proceedings of the Institution of Mechanical Engineers, Part C: Journal of Mechanical Engineering Science, 2008. **222**(7): p. 1321-1327.
29. Wan, Z., et al., *Mesh stiffness calculation using an accumulated integral potential energy method and dynamic analysis of helical gears.* Mechanism and Machine Theory, 2015. **92**: p. 447-463.
30. Abbes, M.S., et al., *Dynamic analysis of helical gears supported by rolling elements bearings.* Journal of Theoretical and Applied Mechanics, 2011. **41**(1): p. 33-50.
31. Gu, X., et al., *Analytical investigations on the mesh stiffness function of solid spur and helical gears.* Journal of Mechanical Design, 2015. **137**(6): p. 063301.
32. Andersson, A. and L. Vedmar, *A dynamic model to determine vibrations in involute helical gears.* Journal of Sound and Vibration, 2003. **260**(2): p. 195-212.
33. Walha, L., et al., *Effect of manufacturing defects on the dynamic behaviour for an helical two-stage gear system.* Mécanique & Industries, 2009. **10**(5): p. 365-376.
34. Zeyin, H., et al., *Parametric modeling and contact analysis of helical gears with modifications.* Journal of Mechanical Science and Technology, 2016. **30**(11): p. 4859-4867.
35. Kar, C. and A. Mohanty, *An algorithm for determination of time-varying frictional force and torque in a helical gear system.* Mechanism and machine theory, 2007. **42**(4): p. 482-496.
36. Kar, C. and A. Mohanty, *Determination of time-varying contact length, friction force, torque and forces at the bearings in a helical gear system.* Journal of Sound and Vibration, 2008. **309**(1): p. 307-319.
37. Jiang, H., *Analysis of time-varying friction excitations in helical gears with refined general formulation.* Proceedings of the Institution of Mechanical Engineers, Part C: Journal of Mechanical Engineering Science, 2015. **229**(13): p. 2467-2483.
38. Jiang, H. and F. Liu, *Dynamic features of three-dimensional helical gears under sliding friction with tooth breakage.* Engineering Failure Analysis, 2016. **70**: p. 305-322.

39. Jiang, H., Y. Shao, and C.K. Mechefske, *Dynamic characteristics of helical gears under sliding friction with spalling defect.* Engineering Failure Analysis, 2014. **39**: p. 92-107.
40. Chang, Q., et al., *Nonlinear Modeling of Helical Gear Pair with Friction Force and Frictional Torque.* WSEAS Transactions on Applied and Theoretical Mechanics, 2014. **9**: p. 264-274.
41. MĄCZAK, J., *Model Based Local Fault Detection in Helical Gears.* Vibrations in Physical Systems Vol.26 (2014).
42. Ding, H., *Dynamic wear models for gear systems*. 2007, PhD Thesis, The Ohio State University.
43. Osman, T. and P. Velex, *Static and dynamic simulations of mild abrasive wear in wide-faced solid spur and helical gears.* Mechanism and Machine Theory, 2010. **45**(6): p. 911-924.
44. Kahraman, A., P. Bajpai, and N. Anderson, *Influence of tooth profile deviations on helical gear wear.* Journal of Mechanical Design, 2005. **127**(4): p. 656-663.
45. Flodin, A. and S. Andersson, *A simplified model for wear prediction in helical gears.* Wear, 2001. **249**(3): p. 285-292.
46. Flodin, A., *Wear of spur and helical gears, Ph.D. Thesis, KTH Stockholm*, in *Royal Institute of Technology, Stockholm*. 2000.
47. Flodin, A. and S. Andersson, *Simulation of mild wear in helical gears.* Wear, 2000. **241**(2): p. 123-128.
48. Kahraman, A.A., NE Bajpai, P, *A surface wear prediction methodology for parallel-axis gear pairs.* Journal of Tribology, ASME, 2004.
49. Kahraman, A.B., P Anderson, NE, *Influence of tooth profile deviations on helical gear wear.* Journal of Mechanical Design, 2005. **127**(4): p. 656-663.
50. Wink, C.H. *Correlation of Tooth Surface Wear Prediction With Experimental Results of Spur and Helical Gears in Commercial Vehicle Transmissions*. in *in 25th International Conference on Design Theory and Methodology; ASME 2013, Power Transmission and Gearing Conference. 2013. Portland, Oregon, USA: American Society of Mechanical Engineers*. 2013. American Society of Mechanical Engineers.
51. Ding, H., *A study of interactions between dynamic behavior of gear systems and surface wear, PhD Thesis*, in *Mechanical Engineering*. 2007, The Ohio State University.
52. Hu, C., Smith, Wade A, Randall, Robert B, Peng, Zhongxiao, *Development of a gear vibration indicator and its application in gear wear monitoring.* Mechanical Systems and Signal Processing, 2016. **76**: p. 319-336.
53. Velex, P. and P. Sainsot, *An analytical study of tooth friction excitations in errorless spur and helical gears.* Mechanism and Machine Theory, 2002. **37**(7): p. 641-658.
54. Velex, P. and V. Cahouet, *Experimental and numerical investigations on the influence of tooth friction in spur and helical gear dynamics.* Journal of Mechanical Design, 2000. **122**(4): p. 515-522.
55. Kubur, M., et al., *Dynamic analysis of a multi-shaft helical gear transmission by finite elements: model and experiment.* Journal of vibration and acoustics, 2004. **126**(3): p. 398-406.
56. Brauer, J. and S. Andersson, *Simulation of wear in gears with flank interference—a mixed FE and analytical approach.* Wear, 2003. **254**(11): p. 1216-1232.
57. He, S., R. Gunda, and R. Singh, *Inclusion of sliding friction in contact dynamics model for helical gears.* Journal of mechanical design, 2007. **129**(1): p. 48-57.
58. Brethee, K.F., et al. *Analysis of frictional effects on the dynamic response of gear systems and the implications for diagnostics*. in *21st International Conference on Automation and Computing (ICAC), 2015, University of Strathclyde, Glasgow, UK*. 2015. IEEE. ISBN 978-0-9926801-0-7
59. Osman, T. and P. Velex, *A model for the simulation of the interactions between dynamic tooth loads and contact fatigue in spur gears.* Tribology International, 2012. **46**(1): p. 84-96.
60. Yesilyurt, I., F. Gu, and A.D. Ball, *Gear tooth stiffness reduction measurement using modal analysis and its use in wear fault severity assessment of spur gears.* NDT and E International, 2003. **36**(5): p. 357-372.
61. Amarnath, M., S. Chandramohan, and S. Seetharaman, *Experimental investigations of surface wear assessment of spur gear teeth.* Journal of Vibration and Control, 2012. **18**(7): p. 1009-1024.

62. Park, D., *Development of surface wear and lapping simulation models for hypoid gears*. 2009, PhD Thesis, The Ohio State University.
63. Park, D., M. Kolivand, and A. Kahraman, *Prediction of surface wear of hypoid gears using a semi-analytical contact model.* Mechanism and Machine Theory, 2012. **52**: p. 180-194.
64. Bajpai, P., A. Kahraman, and N. Anderson, *A surface wear prediction methodology for parallel-axis gear pairs.* Journal of tribology, 2004. **126**(3): p. 597-605.
65. Kumar, A., P. Jain, and P. Pathak. *Study of Tooth Wear on Spur Gear Performance Parameters Using Reverse Engineering*. in *International Conference on Production and Mechanical Engineering (ICPME-2014), Bangkok, Thailand*. 2014.
66. Li, C.-F., et al., *Coupled lateral-torsional-axial vibrations of a helical gear-rotor-bearing system.* Acta Mechanica Sinica, 2014. **30**(5): p. 746-761.
67. Wei, J., et al., *Effects of dynamic transmission errors and vibration stability in helical gears.* Journal of Mechanical Science and Technology, 2014. **28**(6): p. 2253-2262.
68. He, S., R. Gunda, and R. Singh, *Effect of sliding friction on the dynamics of spur gear pair with realistic time-varying stiffness.* Journal of Sound and Vibration, 2007. **301**(3): p. 927-949.
69. Kang, J.S. and Y.-S. Choi, *Optimization of helix angle for helical gear system.* Journal of mechanical science and technology, 2008. **22**(12): p. 2393-2402.
70. Wang, Q., et al., *A Model to Determine Mesh Characteristics in a Gear Pair with Tooth Profile Error.* Advances in Mechanical Engineering, 2015. **6**: p. 751476-751476.
71. Brethee, K.F., F. Gu, and A.D. Ball, *Frictional effects on the dynamic responses of gear systems and the diagnostics of tooth breakages.* Systems Science & Control Engineering, 2016. **4**(1): p. 270-284.
72. Hamel, M.A., *Condition monitoring of helical gears using acoustic emission (AE) technology.* PhD Thesis, Cranfield University, 2013.
73. Xu, H., *Development of a generalized mechanical efficiency prediction methodology for gear pairs*. 2005, PhD Thesis, The Ohio State University.
74. Chaari, F., et al., *Modelling of local damages in spur gears and effects on dynamics response in presence of varying load conditions.* Proceedings of Surveillance 6, UTC Complegne, 2011: p. 1-19.
75. Manwell, J.F., J.G. McGowan, and A.L. Rogers, *Wind energy explained: theory, design and application*. Second Edition ed. 2010: John Wiley & Sons, Ltd, Publication.
76. Zhen, D., et al., *Acoustic measurements for the combustion diagnosis of diesel engines fuelled with biodiesels.* Measurement Science and Technology, 2013. **24**(5): p. 055005.
77. Thompson, R. and W. B. *Gear diagnostics and wear detection*. in *Mechanical Engineering*. 1969. ASME-AMER SOC MECHANICAL ENG 345 E 47TH ST, NEW YORK, NY 10017.
78. Randall, R., *A new method of modeling gear faults.* Journal of Mechanical Design-Trans.ASME104, 1982. **104**(2): p. 259-267.